Attenuation of radio signals by the ionosphere of Mars: Theoretical development and application to MARSIS observations

Paul Withers[1]

Received 10 June 2010; revised 13 December 2010; accepted 29 December 2010; published 11 March 2011.

[1] We investigate the ionospheric conditions required to explain Mars Express Mars Advanced Radar for Subsurface and Ionosphere Sounding topside radar sounder observations of ionospheric attenuation in excess of 13 dB at 5 MHz during solar energetic particle events. We develop theoretical expressions for the attenuation caused by a layer of ionospheric plasma in cases of high, intermediate, and low radio frequency relative to the electron-neutral collision frequency at the ionospheric layer. We apply these relationships to four layers: the M2 layer produced at 120 km by solar extreme ultraviolet photons, the M1 layer produced at 100 km by solar X-ray photons and associated electron impact ionization, the meteoric layer produced at 85 km by meteoroid ablation, and a putative plasma layer produced at 35 km by cosmic rays. Attenuation is weaker in the M2 layer than in the M1 layer. Attenuation in the M1 and meteoric layers are comparable, although their properties are quite variable. The greatest attenuation for radio frequencies above 50 MHz occurs in the predicted plasma layer at 35 km, but its effects are relatively small at lower frequencies. If optimally located with a peak altitude of 50 km, a layer with a peak plasma density of 10^9 m^{-3} is sufficient to explain the observed 13 dB attenuation. Although the electron densities produced by solar energetic particle events at Mars have not been directly simulated, the required electron densities are plausible. However, the altitude at which solar energetic particles produce plasma is uncertain.

Citation: Withers, P. (2011), Attenuation of radio signals by the ionosphere of Mars: Theoretical development and application to MARSIS observations, *Radio Sci.*, *46*, RS2004, doi:10.1029/2010RS004450.

1. Introduction

[2] Ionospheres affect radio navigation and communication systems, as well as radio-based scientific instruments, by their effects on radio wave propagation [e.g., *Ratcliffe*, 1959; *Budden*, 1985; *Hargreaves*, 1992; *Rawer*, 1993; *Reinisch et al.*, 2000; *El-Rabbany*, 2002; *Kliore et al.*, 2004; *Blaunstein and Plohotniuc*, 2008]. Here we investigate how the attenuation of radio signals by the ionosphere of Mars affects topside radar sounders and existing and potential communications systems.

[3] Mars is currently a major target for solar system exploration. At the time of writing, NASA rovers Spirit and Opportunity are conducting surface operations and NASA's Mars Odyssey, ESA's Mars Express, and NASA's Mars Reconnaissance Orbiter are conducting orbital operations [*Crisp et al.*, 2003; *Saunders et al.*, 2004; *Chicarro et al.*, 2004; *Zurek and Smrekar*, 2007]. Planned future missions and their anticipated launch dates include NASA's Mars Science Laboratory rover (2011), Russia's Phobos-Grunt sample return mission (2011), China's Yinghuo-1 orbiter (2011), and NASA's MAVEN orbiter (2013).

[4] Typical missions to the surface of Mars have two communications pathways: a direct-to-Earth link (~5 GHz) and a link between the surface and orbit (400 MHz) [*Roncoli and Ludwinski*, 2002; *Crisp et al.*, 2003]. Typical orbital missions also have these same two communications pathways [*Edwards et al.*, 2003; *Graf et al.*, 2005; *Zurek and Smrekar*, 2007]. The transmission of radio signals through the ionosphere of Mars is therefore common for both surface and orbital missions at Mars. In addition, the operation of radar instruments on orbiters, such as Mars Advanced Radar for Subsurface and Ionosphere Sounding (MARSIS) (0.1–5.4 MHz) on Mars Express [*Picardi et al.*,

[1]Center for Space Physics, Boston University, Boston, Massachusetts, USA.

0048-6604/11/2010RS004450

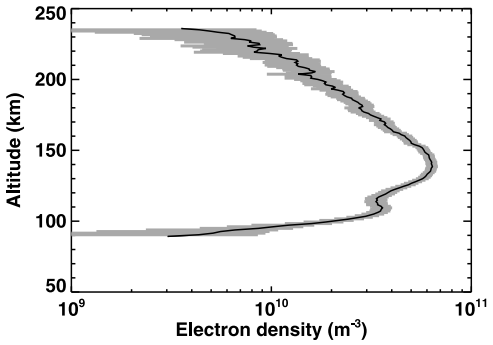

Figure 1. A typical Mars Global Surveyor radio occultation electron density profile, 0337M41A.EDS, with 1σ uncertainties. Note the M2 layer at 140 km and the M1 layer at 110 km.

2004] and SHARAD (15–25 MHz) on Mars Reconnaissance Orbiter [*Seu et al.*, 2004], also involves radio signals passing through the ionosphere of Mars.

[5] The aim of this work is to investigate how the ionosphere of Mars attenuates the signals of such radio systems for a range of possible ionospheric states and a range of radio frequencies. There are two motivating factors behind this work. First, we wish to determine what ionospheric properties are required to explain sporadic failures of the MARSIS instrument to detect the surface of Mars after solar energetic particle events [*Morgan et al.*, 2006, 2010; *Espley et al.*, 2007; *Nielsen et al.*, 2007]. Second, we wish to develop the foundations necessary for future studies of the effects of Martian ionospheric conditions on radio navigation and communication systems at Mars during extreme space weather events [*Foullon et al.*, 2005; *Crosby et al.*, 2008].

[6] The structure of this work is as follows. Section 2 introduces the ionosphere of Mars, the interaction of radio waves with ionospheric plasma, and previous work on the effects of the Martian ionosphere on radio waves. Section 3 develops general expressions for the power lost by a radio signal that propagates through a plasma layer in an unmagnetized ionosphere. Section 4 applies these expressions to four Martian ionospheric layers. Section 5 investigates the ionospheric conditions necessary to explain the strong attenuation observed occasionally by the MARSIS instrument. Section 6 summarizes the findings of this work and Appendix A derives a mathematical relationship that is important for section 3.

2. Background

2.1. The Ionosphere of Mars

[7] The dayside ionosphere of Mars was recently reviewed by *Withers* [2009]. Figure 1 shows a typical electron density profile from the ionosphere of Mars. Figure 2 shows a schematic representation of the main features and forcings associated with the ionosphere of Mars. Solar photons are the main external forcing, but the solar wind's flux of energetic particles and embedded magnetic field affect the topside ionosphere and its boundary with the magnetosheath above. The magnetic environment at Martian ionospheric altitudes is extremely variable, and it is affected by crustal magnetic fields, which vary with position, and the solar wind magnetic field, which varies with position and time. This affects both internal ionospheric processes, such as bulk plasma motion and plasma instabilities, and external forcings, such as the flux of precipitating energetic particles. The ionospheric state clearly depends on magnetic environment to some degree, but the detailed interactions and processes are not currently well understood.

[8] The main layer in the ionosphere, called the M2 layer, is produced by the photoionization of carbon dioxide molecules, the most abundant atmospheric constituent, by solar extreme ultraviolet (EUV) photons. The resultant CO_2^+ ions rapidly charge exchange with neutral oxygen atoms, the next most abundant atmospheric species at ionospheric altitudes, to form longer-lived O_2^+ ions [*Hanson et al.*, 1977; *Chen et al.*, 1978; *Fox*, 2004; *Fox and Yeager*, 2006]. This is the dominant ion species. Since time constants in the M2 layer are much shorter for photochemical processes than for transport processes, the dominant loss process here is the dissociative recombination of O_2^+ ions. As the photoionization cross section for CO_2 is approximately uniform across much of the EUV spectrum [*Schunk*

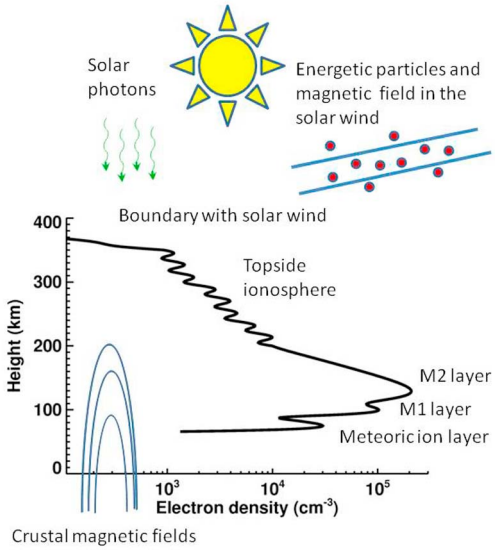

Figure 2. Schematic illustration of the main features and forcings associated with the ionosphere of Mars.

and Nagy, 2000], the M2 layer can be adequately represented as a Chapman layer for many purposes [*Chapman*, 1931a, 1931b]. Several other processes can create additional plasma layers at lower altitudes.

[9] First, a less dense layer, called the M1 layer, is found at 100–110 km altitude, 20 km below the M2 layer [*Bougher et al.*, 2001; *Fox*, 2004; *Mendillo et al.*, 2006]. Some plasma in the M1 layer is produced by photoionization by solar soft X-rays, but the majority is produced by electron impact ionization. Photoionization by a soft X-ray produces a very energetic photoelectron that thermalizes (i.e., its speed reduces to the characteristic thermal speeds of other particles) via collisions with neutral molecules. Electron-neutral collisions may ionize the neutral molecule if the impact energy is sufficiently large, and each photoionization event in the M1 layer leads to the production of ~5–10 ion-electron pairs [*Fox*, 2004; *Nicholson et al.*, 2009]. After CO_2^+ ions are produced in the M1 layer, they follow the same series of photochemical processes as in the M2 layer. Since the solar soft X-ray spectrum is extremely variable, the properties of the M1 layer are also extremely variable [e.g., *Christou et al.* 2007]. This layer is significantly enhanced during solar flares [*Mendillo et al.*, 2006].

[10] Second, a layer attributed to meteoroid influx is sporadically present around 85 km altitude [*Pesnell and Grebowsky*, 2000; *Molina-Cuberos et al.*, 2003; *Pätzold et al.*, 2005; *Withers et al.*, 2008]. The interaction of high-speed meteoroids and atmospheric gases leads to the deposition in the atmosphere of species that would otherwise be absent, such as neutral Mg or Fe. Related ions, such as Mg^+ or Fe^+, are also produced. These ions may be produced directly during meteoroid ablation by the impact ionization of ablated neutral metal atoms in collisions with atmospheric molecules, indirectly by photoionization of neutral metal atoms, or indirectly by charge exchange between neutral metal atoms and atmospheric ions. The photochemical lifetimes of atomic metal ions are measured in hours, much longer than the few minutes of O_2^+ ions, so even a modest production rate can result in substantial plasma densities.

[11] Third, the precipitation of high-energy particles, such as cosmic rays and solar energetic particles, can produce plasma at altitudes below the M2 layer [*Molina-Cuberos et al.*, 2002; *Leblanc et al.*, 2002; *Haider et al.*, 2009; *Brain et al.*, 2009]. This is the only plasma layer discussed in this work where negative ion densities may be significant. In this case, the electron density does not necessarily equal the plasma density. We label the layer of electrons produced by energetic particle precipitation as the "EP" layer. *Molina-Cuberos et al.* [2002] and *Haider et al.* [2009] each simulated a single predicted ionospheric profile produced by cosmic rays with peak electron densities at 35 km. *Leblanc et al.* [2002] reported a modeled vertical profile of energy deposition rate above 80 km during a particular solar energetic particle event, but did not describe ionization rates or resultant plasma densities. Theoretical models of the production of plasma by the precipitation of high-energy particles are relatively unconstrained and immature.

[12] The nightside and dayside ionospheres differ significantly due to the absence of ionizing solar irradiance on the nightside. Nightside electron densities at the altitudes of the M2 and M1 layers, where photochemical lifetimes are on the order of minutes, are much smaller and more variable than on the dayside [*Zhang et al.*, 1990; *Fox et al.*, 1993; *Gurnett et al.*, 2008]. Electron densities as high as 10^{10} m^{-3} at M1 and M2 layer altitudes have been observed at solar zenith angles of 110°, although it is uncertain if these densities are produced by the photoionization processes responsible for these dayside layers or not. The nightside meteoric and EP layers are probably more similar to their dayside counterparts. Atomic metal ions in the meteoric layer have photochemical lifetimes on the order of hours to days [*Withers et al.*, 2008], so this layer is likely to persist onto the nightside [*Pätzold et al.*, 2005]. Plasma in the EP layers is produced by particles, not photons, which are incident on the nightside of Mars. Solar energetic particles can precipitate onto all regions of Mars, not just the dayside, due to their large gyroradius, and the distribution of galactic cosmic rays is relatively isotropic. The ion gyroradius at Mars is comparable to the planetary radius [*Leblanc et al.*, 2002] due to its weak magnetic field. For instance, a 50 keV O^+ ion in a 40 nT magnetic field has a gyroradius of over 3000 km. We expect the meteoric and EP layers, but not the M1 and M2 layers, to be present on the nightside.

[13] The magnetic environment in an ionosphere, especially the magnetic field strength, affects interactions between a radio wave and ionospheric plasma. Unlike Earth or Jupiter, Mars does not possess a strong dipolar magnetic field generated deep within the planetary interior. Instead, it possesses localized regions of magnetic fields generated by remanent magnetism in its crust [*Acuña et al.*, 1999, 2001]. In certain locations, the magnetic field strength at ionospheric altitudes can exceed 1000 nT, as shown in Figure 10 of *Brain et al.* [2003]. Elsewhere, crustal fields are weak or absent. These localized regions of strong field produce unusual magnetic topologies. Magnetic field lines can rotate from vertical to horizontal over distances of a few hundred kilometers, a fraction of the planetary radius. Minimagnetospheres are formed where closed and strong field lines isolate ionospheric plasma from solar wind plasma. Cusp-like conditions prevail on their boundaries, which permit solar wind plasma to flow downward into the ionosphere easily and ionospheric plasma to flow outward easily [*Brain et al.*, 2007]. In order to keep the scope and complexity of this work tractable, we focus on the unmagnetized and weakly

magnetized regions at Mars where the effects of magnetic fields can be neglected. This simplification would not be appropriate on Earth. The following introduction of refractive index and attenuation is therefore less general and comprehensive than is typical for terrestrial applications [e.g., *Rishbeth and Garriott*, 1969; *Budden*, 1985; *Schunk and Nagy*, 2000; *Gurnett and Bhattacharjee*, 2005].

2.2. Interaction of Radio Waves With Ionospheric Plasma

[14] The complex refractive index of an unmagnetized ionosphere, μ_c, in which ion motion is neglected satisfies [*Budden*, 1985]

$$\mu_c^2 = 1 - \frac{\omega_p^2}{\omega(\omega - i\nu)}, \quad (1)$$

where ω_p is the plasma angular frequency, ω is the angular frequency of the electromagnetic wave, i is the square root of -1, and ν is the electron-neutral collision frequency. The plasma angular frequency satisfies $\omega_p^2 = Nq^2/m_e\epsilon_0$ where N is electron density, q is the elementary charge, m_e is the electron mass, and ϵ_0 is the permittivity of free space. Equation (1) follows from equation 4.47 of *Budden* [1985] with $Y = 0$ for an unmagnetized plasma, $X = Nq^2/m_e\epsilon_0\omega^2$, and $U = 1 - i\nu/\omega$. These expressions for Y, X, and U are stated in equations 3.22, 3.5, and 3.16 of *Budden* [1985]. The plasma frequency, f_p, equals $\omega_p/2\pi$ and the electromagnetic wave frequency, f, satisfies $f = \omega/2\pi$. If we define the real and imaginary parts of the complex refractive index by $\mu_c = \mu_r + i\mu_i$, then it follows from equation (1) that

$$\mu_r^4 - \left(1 - \frac{\omega_p^2}{(\omega^2 + \nu^2)}\right)\mu_r^2 - \frac{\omega_p^4\nu^2}{4\omega^2(\omega^2 + \nu^2)^2} = 0. \quad (2)$$

In the collisionless limit where $\nu \ll \omega$ (electron-neutral collision frequency much less than angular frequency of the radio wave), $\mu_r^2 = (1 - \omega_p^2/\omega^2)$. Radio waves with angular frequency ω cannot propagate into regions where $\mu_r^2(\omega) < 0$. If a radio wave encounters a surface where $\mu_r^2 = 0$ (equivalent to $\omega = \omega_p$ in the collisionless limit), then it is reflected at that surface.

[15] We define the real and imaginary parts of the complex wave number k_c by $k_c = k_r + ik_i$, where $k_c = \omega\mu_c/c$ and c is the speed of light. The value of k_i controls how the radio wave amplitude changes due to absorption. If E is radio wave amplitude and s is distance, then $k_i = dE/(E\,ds)$. From equation (1), we have

$$k_i = \frac{-\omega_p^2}{2c\mu_r} \cdot \frac{\nu}{\nu^2 + \omega^2}. \quad (3)$$

The received amplitude, E_r, is related to the transmitted amplitude, E_t, by

$$\frac{E_r}{E_t} = \exp\left(\int k_i ds\right) = \left[\exp\left(\int k_i dz\right)\right]^{\sec(\mathrm{OZA})}, \quad (4)$$

where we have used $ds = \sec(\mathrm{OZA})dz$, z as altitude, OZA as the angle between the ray path and the vertical, and the assumption that the ionosphere can be treated as plane parallel in the regions where its contribution to the attenuation is significant. In the case of an orbiting transmitter and a surface receiver, OZA is the "orbiter zenith angle". The power loss, P, is given in decibels (dB) by

$$\begin{aligned} P(\mathrm{dB}) &= -20\log_{10}(E_r/E_t) \\ &= -20\log_{10}(e)\sec(\mathrm{OZA})\left(\int k_i dz\right), \end{aligned} \quad (5)$$

where $e = \exp(1)$ and the minus sign ensures that the power loss is positive. Equations (3) and (5) show that the effects of multiple plasma layers on the absorption coefficient, k_i, and the power loss, P (dB), are additive if the real part of the refractive index, μ_r, is close to unity ($\omega_p \ll \omega$ for a collisionless ionosphere). For radio waves that are not reflected by any ionospheric layer, the attenuation caused by a multilayered ionosphere can be calculated by studying each individual layer in turn, then adding their respective values of P (dB).

2.3. Previous Work on the Effects of the Martian Ionosphere on Radio Waves

[16] Most existing work on this topic has been motivated by the need to understand the functioning of potential or actual scientific instruments. The frequencies used by past and current communications systems have been high enough that ionospheric effects are relatively small. Current Mars missions use ~5 GHz frequencies for communications with Earth [*Tyler et al.*, 2001] and 400 MHz frequencies for short-range communications [*Edwards et al.*, 2003]. However, future missions, particularly those requiring communications between landed or near-surface explorers, may use lower frequencies that are more affected by the ionosphere. For certain applications, ionospheric effects are beneficial; for example, the reflection of low-frequency radio signals can extend range over the horizon [e.g., *Melnik and Parrot*, 1999]. Terrestrial communications systems with sub-GHz frequencies (http://www.ntia.doc.gov/osmhome/osmhome.html) that might be adapted for Martian use include long-range shortwave radios (~10 MHz), citizens' band (CB) radios (~30 MHz), and cordless telephones (one generation uses 46 MHz frequencies).

[17] *Melnik and Parrot* [1999] investigated the propagation of radio waves in the 10 Hz to 10 kHz range to support radio wave experiments on the Russian Mars 96 and Japanese Nozomi missions (both missions failed). They found that these low frequencies, which might be naturally produced in the lower atmosphere by electrical discharges associated with airborne dust, could only propagate upward to orbital detectors under nightside ionospheric conditions at low solar activity and in the presence of a strong magnetic field. *Witasse et al.* [2001] investigated the effects of meteoric layers on MHz radio signals to support radar experiments on Mars Express and Nozomi. They found that the attenuation could exceed tens of dB.

[18] *Armand et al.* [2003] investigated the distortion of 1–5 MHz radar pulses by the ionosphere and its impact on subsurface radar sounding to support the MARSIS instrument on Mars Express. They found that the ionosphere creates significant pulse distortion at MHz frequencies. *Safaeinili et al.* [2003] developed calibration schemes for the MARSIS instrument in order to understand and correct for several ionospheric effects, including attenuation, Faraday rotation, and pulse dispersion. They predicted attenuation on the order of 1 dB at MHz frequencies under normal dayside ionospheric conditions.

[19] *Mendillo et al.* [2004] investigated ionospheric effects on a hypothetical global positioning system at Mars and found that range errors are on the order of 1 m at 1 GHz. They did not consider the effects of power loss. The range error is proportional to the line-of-sight total electron content (TEC) above the receiver, where the subsolar vertical TEC is approximately 10^{16} m^{-2}. Even during a large solar flare or solar energetic particle event, the vertical TEC is unlikely to exceed twice the value found at the subsolar point under solar maximum conditions.

3. General Expressions for Power Loss

3.1. Basic Assumptions

[20] In this section, we derive some general expressions for the power loss experienced by a radio signal during one-way propagation through an ionosphere. These will be applied to the specific case of Mars in section 4. It is clear from section 2.2 that the study of power loss has two end-member cases ($\omega \gg \nu$ and $\omega \ll \nu$) separated by an intermediate case. We make one significant assumption: that the real part of the refractive index is unity or $\mu_r = 1$. The validity of this assumption, which is clearly reasonable for $\omega_p \gg \omega \gg \nu$, is examined for Mars in section 4. We consider a single ionospheric layer with the shape of a Chapman layer, which is a reasonable approximation for the shape of many ionospheric layers, especially those found on Mars [*Withers*, 2009]. A Chapman layer shape is reasonable for a single layer, not a sum of multiple layers. Our results do not change greatly if a symmetric Gaussian shape is assumed instead. The electron density $N(z)$ satisfies

$$N = N_0 \exp\left(\frac{1}{2}\left(1 - \frac{z - z_0}{L} - \exp\left(-\frac{z - z_0}{L}\right)\right)\right), \quad (6)$$

where N_0 is the maximum electron density, z_0 is the altitude at which $N = N_0$, and L is the width of the layer. Note that we do not require L to equal the neutral scale height, H, at this point. Although we will do so for the Mars-specific results in section 4, we increase the generality of our theoretical results by permitting $L \neq H$ at present. Assuming a uniform composition and acceleration due to gravity, the electron-neutral collision frequency $\nu(z)$ satisfies

$$\nu = \nu_0 \exp\left(-\frac{z - z_0}{H}\right), \quad (7)$$

where ν_0 is the value of ν at $z = z_0$. We define η as the ratio of the width of the ionospheric layer (L) to the neutral scale height (H) so that $\eta = L/H$. We also define x, a dimensionless measure of altitude, as $x = (z - z_0)/L$, which gives $dz = Ldx = \eta H dx$. Therefore,

$$N = N_0 \exp\left(\frac{1}{2}(1 - x - \exp(-x))\right) \quad (8)$$

and

$$\nu = \nu_0 \exp(-\eta x). \quad (9)$$

3.2. High-Frequency Limit ($\omega \gg \nu$)

[21] In this limit, where the angular frequency of the radio wave, ω, is much greater than the electron-neutral collision frequency, ν, equation (3) becomes

$$k_{i,\mathrm{hi}} = \frac{-\omega_p^2 \nu}{2c\omega^2} = \frac{-N_0 q^2 \nu_0}{2m\epsilon_0 c\omega^2} \exp\left(\frac{1}{2}[1 - (1 + 2\eta)x - \exp(-x)]\right). \quad (10)$$

The power loss becomes

$$P_{\mathrm{hi}}(\mathrm{dB}) = 20 \log_{10}(e) \sec(\mathrm{OZA}) \frac{\eta H N_0 q^2 \nu_0}{2m\epsilon_0 c\omega^2} \times \int_{-\infty}^{\infty} \exp\left(\frac{1}{2}(1 - (1 + 2\eta)x - \exp(-x))\right) dx. \quad (11)$$

As shown in Appendix A, the value of the dimensionless integral in equation (11) is $J(1; \eta)$, which equals $\exp(1/2)2^{(\eta+1/2)}\,\Gamma(\eta + 1/2)$ where Γ is the mathematical gamma function. If $\eta = 1$, then $J(1; \eta) = \exp(1/2)\sqrt{2\pi} = 4.133$. With this substitution, we have

$$P_{\mathrm{hi}}(\mathrm{dB}) = 20\log_{10}(e)\sec(\mathrm{OZA})\frac{\eta H N_0 q^2 \nu_0}{2m\epsilon_0 c\omega^2}J(1;\eta). \tag{12}$$

3.3. Low-Frequency Limit ($\omega \ll \nu$)

[22] In this limit, where the angular frequency of the radio wave, ω, is much less than the electron-neutral collision frequency, ν, equation (3) becomes

$$k_{i,\mathrm{lo}} = \frac{-\omega_p^2}{2c\nu} = \frac{-N_0 q^2}{2m\epsilon_0 c\nu_0}\exp\left(\frac{1}{2}[1-(1-2\eta)x-\exp(-x)]\right). \tag{13}$$

Formally, $k_{i,\mathrm{lo}}$ tends to infinity at high altitudes for $\eta > 1/2$ (that is, the ratio of the width of the ionospheric layer, L, to the neutral scale height, H, exceeds 1/2). However, real ionospheres do not have infinite absorption coefficients, k_i, at altitudes high above their ionospheric peak. Since the angular frequency of the radio wave, ω, is constant, but the electron-neutral collision frequency, ν, decreases exponentially with increasing altitude, approximation of equation (3) by equation (13) is formally invalid at high altitudes. Since the attenuation contributed at altitudes many scale heights above the ionospheric layer is negligible, we can continue to use equation (13) at all altitudes if we make additional approximations that eliminate erroneous attenuation from high altitudes.

[23] We first label the altitude where $\omega = \nu$ as z_L, which satisfies

$$z_L = H\ln(\nu_s/\omega), \tag{14}$$

where ν_s is the electron-neutral collision frequency at the surface ($z = 0$). In order for $\omega \ll \nu$ to be satisfied at the ionospheric peak, plasma densities must be negligible at $z > z_L$. Accordingly, we approximate the integral of $k_{i,\mathrm{lo}}$ with respect to altitude as follows:

$$\int_{z=-\infty}^{z=\infty} k_{i,\mathrm{lo}}\,dz = \int_{z=-\infty}^{z=z_L} k_{i,\mathrm{lo}}\,dz. \tag{15}$$

Truncating the integral in this manner prevents the failure of equation (13) at high altitudes from contributing any erroneous attenuation. This leads to

$$\int_{z=-\infty}^{z=z_L} k_{i,\mathrm{lo}}\,dz = \frac{-\eta H N_0 q^2}{2m_e c\epsilon_0\nu_0}\int_{x=-\infty}^{x=x_L} \cdot\exp\left(\frac{1}{2}[1-(1-2\eta)x-\exp(-x)]\right)dx, \tag{16}$$

where x_L, which equals $(z_L - z_0)/\eta H$, is positive. We have not found a general solution to this integral even for the special case where $\eta = 1$ (the width of the ionospheric layer, L, equals the neutral scale height, H). However, an approximate solution can be obtained. The integrand in equation (16) can be separated into the product of two terms, $\exp(0.5 + (\eta - 0.5)x)$ and $\exp(-0.5\exp(-x))$. The second term is close to unity for $x > 0$ and can be neglected. Therefore,

$$\int_{z=-\infty}^{z=\infty} k_{i,\mathrm{lo}}dz \approx \frac{-\eta H N_0 q^2}{2m_e c\epsilon_0\nu_0} \times\left[\int_{x=-\infty}^{x=0}\exp\left(\frac{1}{2}(1-(1-2\eta)x-\exp(-x))\right)dx + \int_{x=0}^{x=x_L}\exp\left(\frac{1}{2}(1-(1-2\eta)x)\right)dx\right]. \tag{17}$$

The term in square brackets is simply a dimensionless scaling factor that relates the power loss to the key physical parameters (η, H, N_0, ν_0). The first dimensionless term inside the square brackets has no obvious analytical solution. Its value depends on η only, so we represent it by the function $\gamma(\eta)$. The function $\gamma(\eta)$ decreases monotonically with increasing η. At $\eta = 1$ (the width of the ionospheric layer, L, equals the neutral scale height, H), $\gamma = 0.689$. The value of γ is on the order of unity for $\eta < 6$, which means that it can be replaced by 1 for all but the broadest of layers without explicit calculation. The second dimensionless term inside the square brackets has a simple solution. Accordingly, equation (17) becomes

$$\int_{z=-\infty}^{z=\infty} k_{i,\mathrm{lo}}\,dz \approx \frac{-\eta H N_0 q^2}{2m_e c\epsilon_0\nu_0} \times\left[\gamma(\eta) - \frac{2}{(1-2\eta)}\exp(0.5) \cdot\left(\exp\left(\frac{-(1-2\eta)x_L}{2}\right)-1\right)\right]. \tag{18}$$

Thus,

$$P_{\mathrm{lo}}(\mathrm{dB}) = 20\log_{10}(e)\sec(\mathrm{OZA})\frac{\eta H N_0 q^2}{2m_e c\epsilon_0\nu_0} \times \left[\gamma(\eta) - \frac{2}{(1-2\eta)}\exp(0.5) \cdot \left(\exp\left(\frac{-(1-2\eta)x_L}{2}\right) - 1\right)\right]. \quad (19)$$

3.4. Intermediate Frequencies

[24] Sometimes neither $\omega \gg \nu$ (section 3.2) nor $\omega \ll \nu$ (section 3.3) is satisfied at all altitudes with appreciable plasma densities. In such cases, neither equation (12) nor equation (19) will provide an accurate estimate of the power loss. Here we state without proof an expression for the power loss at intermediate frequencies. We show in section 4 that this expression is appropriate for Mars.

[25] Recall that z_L is the altitude where $\omega = \nu$. The peak altitude (z_0) at which $(z_0 - z_L) = -\eta H = -L$ is significant here and we label the value of P_{lo} (equation (19)) at this altitude as P^*_{lo}. If the peak altitude (z_0) is more than one layer width below z_L, then the low-frequency limit for the power loss can be used. If z_0 is small enough that $(z_0 - z_L)/\eta H \leq -1$ then $P = P_{\mathrm{lo}}$ from equation (19). If z_0 is larger than this and $(z_0 - z_L)/\eta H > -1$ then P equals the smaller of P^*_{lo} and P_{hi} (equation (12)). Therefore,

$$P = P_{\mathrm{lo}} \text{ if } (z_0 - z_L)/\eta H \leq -1$$
$$P = \text{minimum}\left[P^*_{\mathrm{lo}}, P_{\mathrm{hi}}\right] \text{ if } (z_0 - z_L)/\eta H > -1. \quad (20)$$

As a rough rule of thumb, P equals P^*_{lo} for the altitude range $1 > (z_0 - z_L)/\eta H > -1$ and P_{hi} for the altitude range $(z_0 - z_L)/\eta H > 1$.

[26] The value of P^*_{lo} can be estimated as follows. At $(z_0 - z_L) = -\eta H$, $\nu_0 = e\omega$ and, for $\eta = 1$, the value of the term in square brackets in equation (19) is close to e. Hence,

$$P^*_{\mathrm{lo}}(\mathrm{dB}) = 20\log_{10}(e)\sec(\mathrm{OZA})\left(\frac{HN_0 q^2}{2m_e c\epsilon_0\omega}\right). \quad (21)$$

A sense of the numerical value of P^*_{lo} can be obtained by replacing H, N_0, and f with representative values of 10 km, 10^9 m^{-3}, and 100 MHz, respectively. Hence,

$$P^*_{\mathrm{lo}}(\mathrm{dB}) = 0.73\sec(\mathrm{OZA})\left(\frac{H}{10\text{ km}}\right)\left(\frac{N_0}{10^9\mathrm{m}^{-3}}\right) \cdot \left(\frac{f}{100\text{ MHz}}\right)^{-1}. \quad (22)$$

This is equivalent to the attenuation produced by a uniform layer of electron density N_0 and width $2H$ at an altitude where $\nu/(\nu^2 + \omega^2)$ equals its maximum value of $1/2\omega$ (equation (3)). Thus, attenuation in excess of 1 dB can be produced at MHz frequencies by even a weak plasma layer whose peak density is less than 1% of the subsolar peak electron density in the M2 layer (2×10^{11} m^{-3}) if the plasma layer is located at the optimal altitude. Measurable attenuation, even on the nightside, does not necessarily require large electron densities, which has implications that will be explored in section 5. Having developed approximate analytical formulae for the power loss at all frequencies, albeit with the assumption that $\mu_r = 1$, we now show that they are reasonable for Mars.

4. Application to Mars

4.1. Model of the Atmosphere of Mars

[27] The neutral atmosphere of Mars can be represented as an ideal gas of pure CO_2 with uniform temperature, T, of 150 K and uniform gravitational acceleration, g, of 3.7 m s^{-2} [*Owen*, 1992; *Zurek et al.*, 1992]. This leads to a uniform neutral scale height, H, of 7.6 km. Specifying the surface pressure, p_s, to be 600 Pa determines the neutral density at all altitudes [*Zurek et al.*, 1992]. The electron-neutral collision frequency, ν, equals ϕn where n is neutral number density and ϕ, a momentum transfer coefficient, is 10^{-13} m^3 s^{-1} for CO_2 [*Hake and Phelps*, 1967; *Nielsen* et al., 2007]. The value of ϕ equals the product of the electron thermal speed and the electron-neutral collision cross section [*Gurnett and Bhattacharjee*, 2005]. Both of these factors depend on temperature. However, Figure 13 of *Hake and Phelps* [1967] shows that the temperature dependence of ϕ is relatively small, so we assume a constant value for this exploratory survey. Note that a wide range of values of ϕ have been used in previous work [*Melnik and Parrot*, 1999; *Witasse et al.*, 2001; *Safaeinili et al.*, 2003]. Some previous workers adopted the terrestrial (N_2/O_2) value for ϕ, which is 2 orders of magnitude smaller than the value in the CO_2 atmosphere of Mars [*Nielsen et al.*, 2007]. This should be considered when comparing results.

4.2. Example of Power Loss Using 5 MHz Radio Waves

[28] We assumed that the layer width equalled the neutral scale height ($\eta = 1$) and calculated the power loss as a function of N_0 and z_0 for vertical radio wave propagation (that is, an OZA of 0°) and $f = 5$ MHz, where this frequency was chosen in order to support interpretation of MARSIS observations in section 5. Results are shown in Figure 3. Two separate results are

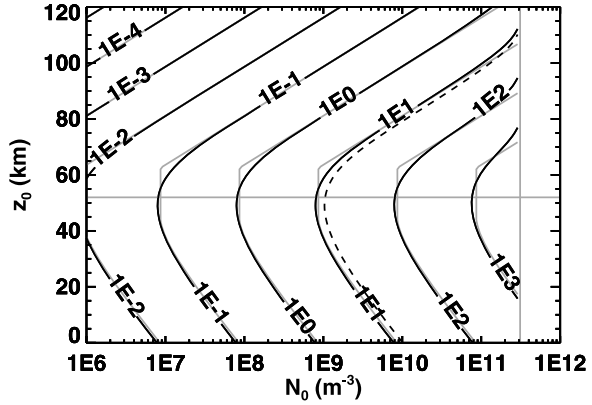

Figure 3. Power loss (dB) in an ionospheric layer as a function of peak electron density, N_0, and altitude, z_0, for $f = 5$ MHz and layer width equal to the neutral scale height. Black contours show the results of a numerical integration. Grey contours show the analytical approximations derived in section 3. Grey contours may be invisible beneath black contours when the approximations are very accurate. In such instances, the grey contours can be seen beneath the numbers that label the black contours. Contours with very small power losses are shown to illustrate the functional dependencies of the results plotted here, not because a power loss of 10^{-4} dB has great practical significance. The dashed black curve indicates the 13 dB contour (section 5). The horizontal grey line indicates z_L, the value of z where $\nu = \omega$, which is the boundary between the high-frequency and low-frequency limits. The vertical grey line indicates the value of N_0 at which the maximum plasma frequency, $f_{p,max}$, equals the radio frequency, f.

shown: black contours represent numerical integration of equation (5) using the comprehensive expressions for the absorption coefficient, k_i, and the real part of the refractive index, μ_r, from equations (2) and (3), and grey contours represent the analytic approximations developed in section 3. The approximations are reasonably accurate for all frequencies. At low peak plasma frequencies (low N_0), the black and grey contours are distinguishable from each other only at peak altitudes where the intermediate expression of section 3 applies (that is, where $z_0 \approx z_L$). As the peak plasma frequency approaches the radio frequency (that is, as N_0 increases), differences between the black and grey contours become more apparent as the assumption that $\mu_r = 1$ weakens. Yet the weakening of this assumption does not have terrible consequences. For regions of Figure 3 where the radio frequency is greater than two times the maximum plasma frequency, the value of the real part of the refractive index, μ_r, differs from unity by less than 0.13.

Table 1. Typical Heights and Electron Densities of Ionospheric Layers Considered in This Work

Layer	Height (km)	Electron Density (m^{-3})
M2	120	2×10^{11}
M1	100	1×10^{11}
Meteoric	85	2×10^{10}
EP	35	1×10^{8}

4.3. Power Losses due to Four Ionospheric Layers

[29] We consider four ionospheric layers, the M2 layer at 120 km [*Withers*, 2009], the M1 layer at 100 km [*Fox*, 2004; *Pätzold et al.*, 2005; *Mendillo et al.*, 2006; *Fox and Yeager*, 2006], the meteoric layer at 85 km [*Pätzold et al.*, 2005; *Withers et al.*, 2008] and the putative EP layer at 35 km [*Molina-Cuberos et al.*, 2002; *Haider et al.*, 2009], and vertical radio wave propagation (OZA=0). Layer heights and electron densities are listed in Table 1. The assumption that the layer width is equal to the neutral scale height ($\eta = 1$) is reasonable for all these layers. For each layer, we consider radio frequencies between 1 MHz and 100 GHz (section 2.3) and peak electron densities between 10^6 m^{-3} and 10^{12} m^{-3}.

4.3.1. Power Loss due to the M2 Layer

[30] The high-frequency limit for power loss can be used here because $\omega > \nu$ at 120 km for all frequencies greater than 660 Hz. The power loss due to the M2 layer is shown in Figure 4. Two separate results were calculated,

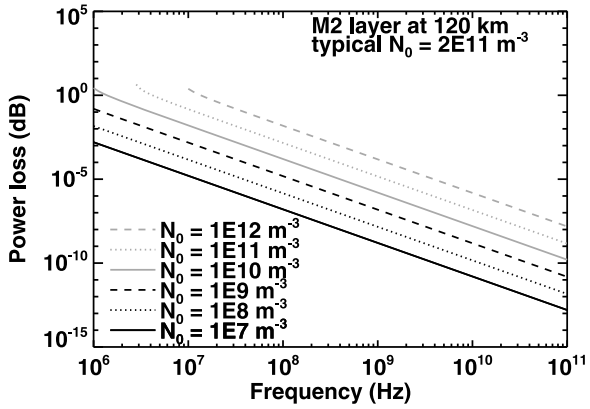

Figure 4. Power loss (dB) in the M2 layer (120 km) as a function of peak electron density, N_0, and radio frequency. Results of a numerical integration, not the analytical approximations derived in section 3, are shown here. Note that some contours do not extend to low frequencies. Radio signals at these frequencies are reflected by the ionosphere before they can reach the surface. Radio waves cannot propagate through the ionosphere if the angular frequency of the radio wave is smaller than the maximum value of the ionospheric plasma frequency.

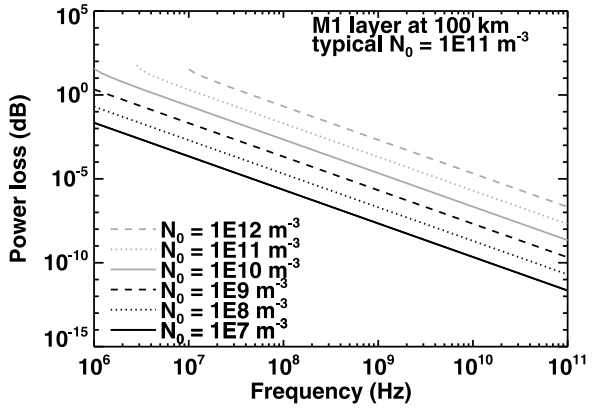

Figure 5. As in Figure 4 but for the M1 layer (100 km).

one for numerical integration and one for the analytical approximations of section 3, but only those for numerical integration are shown here. However, the results are indistinguishable, except where the radio frequency is close to the maximum plasma frequency. For regions where the radio frequency is greater than two times the maximum plasma frequency, the value of μ_r differs from unity by less than 0.13, confirming that the key assumption of section 3 is valid here. The typical subsolar peak electron density of the M2 layer is 2×10^{11} m^{-3} [*Withers*, 2009], so the subsolar power loss exceeds 1 dB only for frequencies below 6 MHz.

4.3.2. Power Loss due to the M1 Layer

[31] The high-frequency limit for power loss can be used here because $\omega > \nu$ at 100 km for all frequencies greater than 9 kHz. The power loss due to the M1 layer is shown in Figure 5. Two separate results were calculated, one for numerical integration and one for the analytical approximations of section 3, but only those for numerical integration are shown here. However, the results are indistinguishable, except where the radio frequency is close to the maximum plasma frequency. For regions where the radio frequency is greater than two times the maximum plasma frequency, the value of μ_r differs from unity by less than 0.13, confirming that the key assumption of section 3 is valid here. The typical peak electron density in the M1 layer is one-third to one-half of the peak electron density in the M2 layer [*Fox and Yeager*, 2006; *Withers*, 2009]. If we assume $N_0 = 10^{11}$ m^{-3}, then the subsolar power loss exceeds 1 dB only for frequencies below 16 MHz. The attenuation caused by the M1 layer exceeds that caused by the subsolar M2 layer if N_0 in the M1 layer is greater than about 2×10^{10} m^{-3}, or one-fifth of our adopted value of 10^{11} m^{-3}. Thus, the ionospheric attenuation experienced during typical conditions is dominated by the M1 layer, not the M2 layer. Electron densities in this layer are significantly enhanced by solar flares, which may lead to $N_0 > 10^{11}$ m^{-3} for short intervals. We defer the study of the rise and fall of attenuation during an intense solar flare to future work.

4.3.3. Power Loss due to the Meteoric Layer

[32] The high-frequency limit for power loss can be used here because $\omega > \nu$ at 85 km for all frequencies greater than 66 kHz. The power loss due to the meteoric layer is shown in Figure 6. Two separate results were calculated, one for numerical integration and one for the analytical approximations of section 3, but only those for numerical integration are shown here. However, the results are indistinguishable, except where the radio frequency is close to the maximum plasma frequency. For regions where the radio frequency is greater than two times the maximum plasma frequency, the value of μ_r differs from unity by less than 0.13, confirming that the key assumption of section 3 is valid here. Note that Figure 6 is consistent with the results of *Witasse et al.* [2001]. The largest electron densities observed in the meteoric layer to date are 2×10^{10} m^{-3} [*Pätzold et al.*, 2005; *Withers et al.*, 2008]. Using this value for N_0 means the power loss exceeds 1 dB only for frequencies below 18 MHz. The attenuation caused by the meteoric layer exceeds that caused by the subsolar M2 layer if N_0 is greater than about 3×10^9 m^{-3}, which is smaller than all peak meteoric densities yet reported [*Pätzold et al.*, 2005; *Withers et al.*, 2008]. If the meteoric layer is present, then its effects on ionospheric attenuation of radio signals are comparable to those of the larger M1 layer and greater than those of the M2 layer.

[33] *Nielsen et al.* [2007] found identical attenuation for the M1 layer at 110 km with peak density of 6×10^{10} m^{-3} and the meteoric layer at 90 km with peak density of 8×10^9 m^{-3}. Equation (12) predicts that the attenuation of these two layers will be identical if the product of the neutral and plasma densities at their peaks

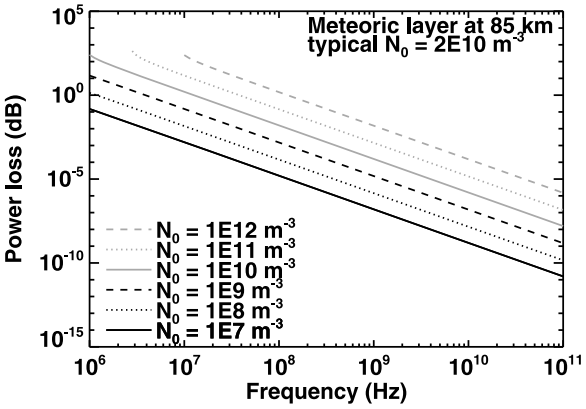

Figure 6. As in Figure 4 but for the meteoric layer (85 km).

are identical. From the equivalence of these two attenuations, equation (12) predicts that the neutral scale height is 10 km, which is exactly the value that was used by *Nielsen et al.* [2007]. This successful prediction shows that the relationships derived in section 3 are consistent with the results of *Nielsen et al.* [2007].

4.3.4. Power Loss due to the EP Layer

[34] At the altitude of the EP layer (z_0 = 35 km), $\omega = \nu$ at 46 MHz. Thus, the high-, intermediate-, and low-frequency cases must be considered here, rather than just a single case. The power loss due to the EP layer is shown in Figure 7. Two separate results were calculated, one for numerical integration and one for the analytical approximations of section 3, but only those for numerical integration are shown here. The curvature visible in Figure 7, which is not present in Figures 4–6, appears because the frequency range of 1 MHz to 100 GHz spans the high-, intermediate-, and low-frequency cases. Only the high-frequency case is relevant for Figures 4–6. The transition between high-, intermediate-, and low-frequency cases is more clearly visible in Figure 8, where results for both numerical integration and the analytical approximations of section 3 are shown. The two sets of results are indistinguishable, except where the radio frequency is close to the maximum plasma frequency and between f = 100 MHz and f = 400 MHz ($\omega = 2 \times$ to $8 \times \nu_0$). For regions where the radio frequency is greater than two times the maximum plasma frequency, the value of μ_r differs from unity by less than 0.06, confirming that the key assumption of section 3 is valid here. There are no direct observations of this layer or its maximum electron density, but two independent models predict that electron densities of 10^8 m^{-3} are produced at 35 km by typical galactic cosmic ray fluxes [*Molina-Cuberos et al.*, 2002; *Haider et al.*, 2009]. Using this value for N_0 means the power loss exceeds 1 dB only for frequencies below 4 MHz. Even at as low a frequency as 1 MHz, the power loss is only 3 dB. The attenuation caused by this plasma layer exceeds that caused by the M2 layer, the M1 layer, and the meteoric layer for all frequencies greater than 50 MHz (Figure 9).

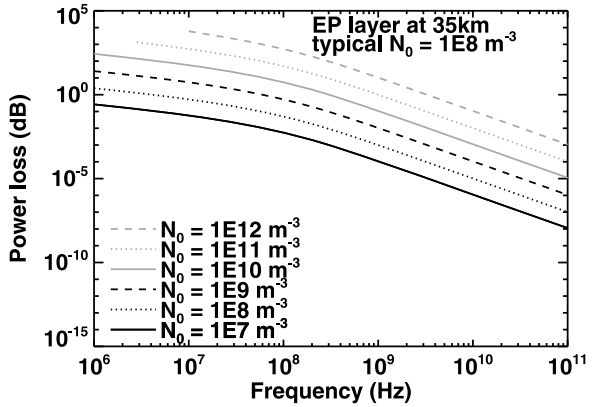

Figure 7. As in Figure 4 but for the EP layer (35 km).

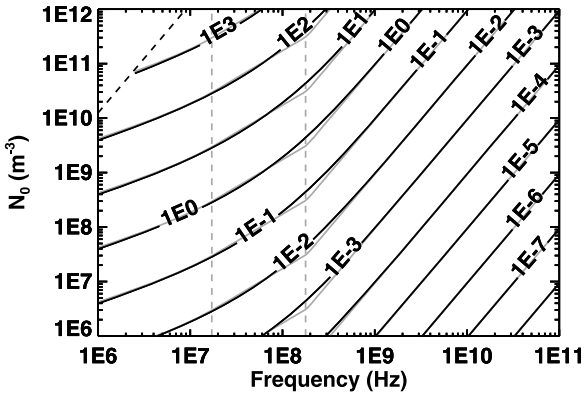

Figure 8. Power loss (dB) in the EP layer (35 km) as a function of peak electron density, N_0, and radio frequency. Black contours show the results of a numerical integration. Grey contours show the analytical approximations derived in section 3. Grey contours may be invisible beneath black contours when the approximations are very accurate. In such instances, the grey contours can be seen beneath the numbers that label the black contours. The dashed black curve indicates where the maximum plasma frequency equals the radio frequency, f. In the region to the left of both vertical grey dashed lines, the grey contours use the low-frequency expression of section 3. In the region between the two vertical grey dashed lines, the grey contours use the intermediate-frequency expression of section 3. In the region to the right of both vertical grey dashed lines, the grey contours use the high-frequency expression of section 3.

5. Application to Attenuation Observed by MARSIS

5.1. MARSIS Observations and Blackouts

[35] The MARSIS topside radar sounder instrument on Mars Express has provided direct measurements of the attenuation of radio signals by the ionosphere of Mars [*Gurnett et al.*, 2008]. This radar, which operates at 0.1 to 5.4 MHz, usually detects surface reflections at frequencies greater than the ionosphere's plasma frequency, but sometimes it does not. The M2 and M1 layers cannot be responsible for the MARSIS blackouts, which persist deep into the nightside where these layers are absent. The spatial patchiness of observed meteoric layers [*Pätzold et al.*, 2005; *Withers et al.*, 2008] is inconsistent with the global scale of the MARSIS blackouts. Blackouts, while they last, are continuous, whereas meteoric layers occur

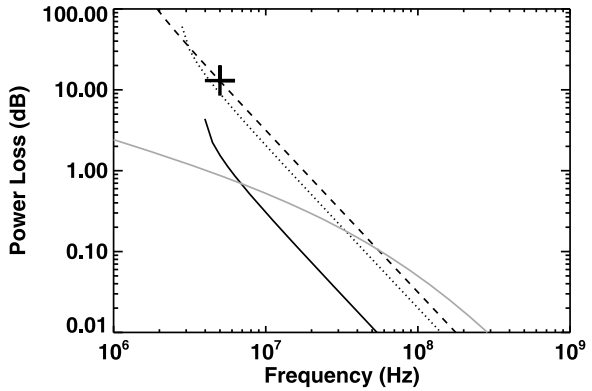

Figure 9. Power loss as a function of frequency for the M2 (black solid line), M1 (black dotted line), meteoric (black dashed line), and EP (grey solid line) layers. The cross indicates the 13 dB of attenuation at 5 MHz required for MARSIS blackouts (section 5).

sporadically. Thus, the M2, M1 and meteoric layers cannot be responsible for these MARSIS blackouts. These "blackout periods" correspond to the duration of solar energetic particle events [*Morgan et al.*, 2006, 2010; *Espley et al.*, 2007]. The flux of galactic cosmic rays, which produce the EP layer, will not rise and fall significantly during solar energetic particle events, and, as discussed below, the EP layer's predicted attenuation is an order of magnitude too small to cause the observed blackouts. Thus, galactic cosmic rays are not responsible for the observed blackouts either.

[36] An example of this phenomenon is shown in Figure 10. Other examples can be seen in Figure 2 of *Gurnett et al.* [2005], Figure 1 of *Morgan et al.* [2006], and Figure 1 of *Espley et al.* [2007] (MARSIS subsurface mode). The lack of a surface reflection in Figure 10 (middle), despite observing conditions that are very similar to those of Figures 10 (top) and 10 (bottom), implies a period of greater than usual attenuation of radio waves in the ionosphere. The elevated attenuation during these observed blackouts has been attributed to greater than usual electron densities below 120 km, although the actual electron densities and altitudes responsible have not been determined. These blackouts may be the first indirect observational evidence for the production of low altitude plasma layers by energetic particles.

5.2. Required Attenuation

[37] The one-way attenuation necessary for surface reflections to be undetectable by MARSIS is about 13 dB [*Nielsen et al.*, 2007]. Figure 9 compares the required power loss at 5 MHz to the power lost in the subsolar M2, subsolar M1, meteoric and EP layers. The predicted power losses for the subsolar M2, subsolar M1, meteoric, and EP layers are 1.5, 9.0, 12.8, and 0.9 dB, respectively. Under normal conditions, MARSIS is not able to observe a surface reflection for solar zenith angles less than 50° [*Morgan et al.*, 2006; *Nielsen et al.*, 2007; *Espley et al.*, 2007]. Neglecting the sporadic meteoric layers and poorly constrained EP layer, the predicted total attenuation is 10.5 dB at the subsolar point. This decreases with increasing solar zenith angle as the peak electron densities in the M1 and M2 layers decrease in a Chapman-like manner. At 50° solar zenith angle, where the observed attenuation is typically 13 dB, the predicted attenuation is approximately 8 dB. Considering the simplified representations of the M2 and M1 layers and the neutral atmosphere in our calculations, and the neglect of possible persistent meteoric layers weaker than the detection limit of radio occultation experiments, the predicted 8 dB is acceptably close to the required 13 dB.

[38] Figure 3 shows how the smallest peak electron density necessary to produce the required 13 dB attenuation at 5 MHz depends on peak altitude. These calculations

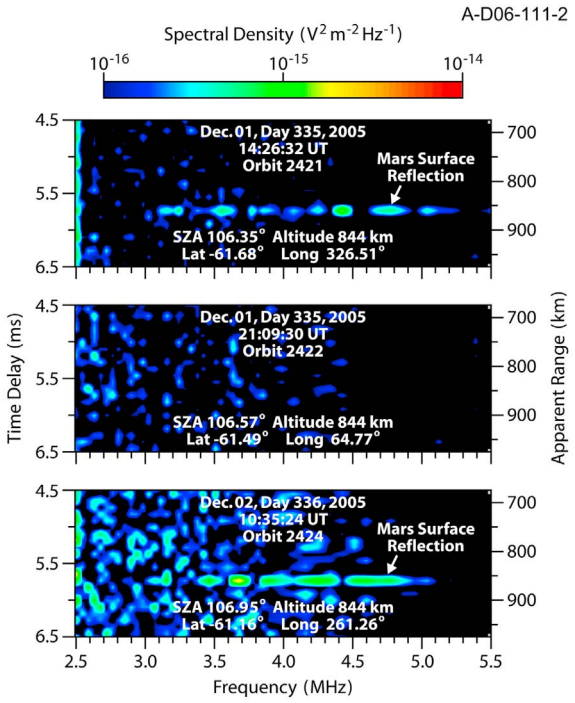

Figure 10. Sample ionograms before, during, and after a MARSIS blackout on 1–2 December 2005. The spacecraft altitude is about 850 km. Longitude is given in °W, and latitude is given in °N. This particular blackout was attributed to the passage of a corotating interaction region at Mars. Previously published as Figure 1 of *Morgan et al.* [2010], with permission from Elsevier.

used a single plasma layer whose width equals the scale height. A layer with a peak plasma density of 10^9 m^{-3} is sufficient to explain the observed attenuation if optimally located with a peak altitude of 50 km. A layer with a peak plasma density of 10^{10} m^{-3} is sufficient to explain the observed attenuation for all peak altitudes below 80 km. A layer with a peak plasma density of 10^{11} m^{-3} is sufficient to explain the observed attenuation for all peak altitudes below 100 km. Since 13 dB is only the lower limit on the actual attenuation during a blackout, greater attenuation is likely at the peak of a solar energetic particle event, which will require even greater electron densities than those indicated by Figure 3. We now turn our attention to whether the peak densities and altitudes implied by Figure 3 are reasonable for ionospheric conditions during a solar energetic particle event. We do not explicitly address the issue of layer width, save to note that wider layers will produce greater attenuation for a given peak density.

5.3. Ionospheric Effects of Solar Energetic Particle Events

[39] Solar energetic particles, whose flux and energy spectrum varies greatly with time, may produce plasma at low altitudes [*Leblanc et al.*, 2002; *Brain et al.*, 2009]. In the single event simulated by *Leblanc et al.* [2002], the energy deposition rate per unit volume, which is likely to be approximately proportional to the ionization rate per unit volume, was greatest at 90–100 km. *Brain et al.*, [2009] found a similar peak altitude for the energy deposition rate per unit volume for their selected solar energetic particle event. Lower peak altitudes might occur if spectra from different solar energetic particle events were studied. Hence, the simulated peak altitudes of 90–100 km do not necessarily mean that all real solar energetic particle events produce plasma layers at such altitudes. Although no models have yet reported simulated Martian electron density profiles produced during solar energetic particle events, we can estimate what electron densities are produced by the energy deposition rates reported by *Leblanc et al.* [2002]. The peak energy deposition rate is 3×10^5 eV cm^{-3} s^{-1}. If we assume that all this energy is used to create ion-electron pairs and the creation of one ion-electron pair requires 35 eV [*Rees and Jones*, 1973], then the ion production rate is about 9000 cm^{-3} s^{-1}. If all ions are rapidly converted into O_2^+ ions, whose loss rate is the product of the dissociative recombination coefficient (2×10^{-7} cm^3 s^{-1}) and the square of the plasma density, then the peak electron density is the square root of the ratio of the production rate and dissociative recombination coefficient [*Rishbeth and Garriott*, 1969] or 2×10^{11} m^{-3}, the same as the subsolar peak density in the M2 layer. Since it is unlikely that all energy goes directly into ionizing the atmosphere, this is probably an overestimate. Nevertheless, this estimate indicates that significant ionization may result from solar energetic particle events. Simulations of Martian electron density profiles produced during solar energetic particle events are needed for further progress. In particular, we cannot draw conclusions about the lowest frequency for which the degradation of radio communications by ionospheric attenuation during large solar energetic particle events is minor until such simulations are performed.

[40] This analysis has led to a paradox. If the peak altitude is above ~80 km, consistent with *Leblanc et al.* [2002] and *Brain et al.* [2009], then the unusually large bottomside electron densities required to explain the MARSIS blackouts should have been observed by radio occultation experiments. Yet radio occultation experiments have not reported such phenomena. If the peak altitude is below ~80 km, which is inconsistent with *Leblanc et al.* [2002] and *Brain et al.* [2009], then the lack of reported detections by radio occultation experiments is not unreasonable.

[41] There are several possible resolutions. First, peak altitudes are above ~80 km, but the lack of reported detections by radio occultation experiments is due to no previous workers carefully examining data obtained during solar energetic particle events. Second, the energy spectra of the solar energetic particles events that caused MARSIS blackouts differ significantly from those used by *Leblanc et al.* [2002] and *Brain et al.* [2009], leading to significantly lower altitudes of maximum energy deposition rate. Third, unusual ionospheric chemistry might lead to ionospheric electron densities not being approximately proportional to the energy deposition rate.

5.4. Testability of Predictions

[42] Modelers can use the tools developed in this work to quickly establish whether or not their predictions of electron density profiles caused by solar energetic particle events can explain the observed MARSIS blackouts, thereby testing whether or not these predicted electron density profiles are realistic. Previous work on MARSIS surface reflections has used a binary detectable/undetectable classification scheme. Yet the ionospheric attenuation can be directly measured as a function of time and frequency using the strength of detectable surface reflections. Such measurements would enable novel scientific investigations of the ionosphere of Mars.

[43] Another data set that might be relevant here is the time history of the signal strength of direct-to-Earth communications at GHz frequencies by landers on the surface of Mars and of surface-to-orbit communications at 400 MHz. It is possible that unusual decreases in signal strength have been observed, even at such high frequencies, during intense solar energetic particle events on Mars. Although attenuation at such high frequencies will be weak, the

Deep Space Network has excellent sensitivity to small changes in signal amplitude.

6. Conclusions

[44] We have obtained general algebraic expressions for the attenuation caused by a layer of ionospheric plasma that has a Chapman layer shape under the assumption that the real refractive index equals unity. The basic functional dependencies are apparent from inspection of the equation that defines the absorption coefficient (equation (3)), but the constants of proportionality are not. Also nontrivial is the smooth transition between expressions for high, intermediate, and low radio frequencies. These expressions have been applied to a model of the ionosphere of Mars, specifically to the M2 layer produced at 120 km by solar extreme ultraviolet photons, the M1 layer produced at 100 km by solar X-ray photons and associated electron impact ionization, the meteoric layer produced at 85 km by meteoroid ablation, and a putative plasma layer produced at 35 km by galactic cosmic rays. The high-frequency limit applies for the M2, M1 and meteoric layers for radio frequencies above 1 MHz. Attenuation is weaker in the M2 layer than in the M1 layer. Attenuation in the M1 and meteoric layers are comparable, although the properties of both layers are quite variable. The greatest attenuation for radio frequencies above 50 MHz occurs in the putative EP layer at 35 km, but its effects are relatively small at lower frequencies.

[45] These expressions have been used to constrain the ionospheric conditions required to explain the absence of surface reflections in MARSIS observations during solar energetic particle events. The electron densities that are required to cause 13 dB of attenuation at 5 MHz and thereby obscure MARSIS surface reflections, which were shown in Figure 3, are plausible, but uncertainty remains in the altitude at which this excess plasma is found. Theoretical models suggest altitudes of 80–100 km, but enhanced plasma density at these altitudes should have been observed by radio occultation experiments. Partial validation of our expressions is provided by the lack of surface reflections in MARSIS observations for solar zenith angles less than 50°, which implies attenuation by 13 dB at 5 MHz and a solar zenith angle of 50°. We predict attenuation of 10.5 dB at the subsolar point and 8 dB at a solar zenith angle of 50°. The observed attenuation of 13 dB and the predicted attenuation of 8 dB are acceptably close, given the simplified atmospheric and ionospheric model used in this work.

[46] The frequencies that can propagate through the ionosphere during solar disturbances without substantial attenuation cannot be found until the ionospheric effects of precipitating solar energetic particles are better understood. Specifically, the resultant electron density profile is needed. This uncertainty is a challenge for the designers of radio navigation and communications systems on future Mars spacecraft.

Appendix A: $J(n; \eta)$

[47] We define $J(n; \eta)$ as

$$J(n;\eta) = \int_{x=-\infty}^{x=\infty} \exp\left(\frac{n}{2}(1 - x - \exp(-x))\right) \exp(-\eta x)\, dx, \tag{A1}$$

where $n > 0$ and $\eta \geq 0$ (section 3.2). Rearranging gives

$$J(n;\eta) = \exp\left(\frac{n}{2}\right) \int_{x=-\infty}^{x=\infty} \exp\left(-\left(\frac{n+2\eta}{2}\right)x\right) \cdot \exp\left(\frac{-n\exp(-x)}{2}\right) dx. \tag{A2}$$

We define y by

$$y = \frac{n\exp(-x)}{2}. \tag{A3}$$

Hence, $x = -\infty$ becomes $y = \infty$, $x = \infty$ becomes $y = 0$, $\exp\left(-\left(\frac{n+2\eta}{2}\right)x\right) = \left(\frac{2y}{n}\right)^{\frac{n+2\eta}{2}}$, $\exp\left(\frac{-n\exp(-x)}{2}\right) = \exp(-y)$, and $dy = -y\, dx$. With these substitutions, equation (A2) becomes

$$J(n;\eta) = \exp\left(\frac{n}{2}\right) \int_{y=0}^{y=\infty} \left(\frac{2y}{n}\right)^{\frac{n+2\eta}{2}} \exp(-y)\, \frac{dy}{y} \tag{A4}$$

$$J(n;\eta) = \exp\left(\frac{n}{2}\right) \left(\frac{2}{n}\right)^{\frac{n+2\eta}{2}} \int_{y=0}^{y=\infty} y^{\frac{n+2\eta-2}{2}} \exp(-y)\, dy. \tag{A5}$$

[48] We define r by

$$y = r^2. \tag{A6}$$

Hence, $y = 0$ becomes $r = 0$, $y = \infty$ becomes $r = \infty$, $y^{\frac{n+2\eta-2}{2}} = r^{(n+2\eta-2)}$, $\exp(-y) = \exp(-r^2)$, and $dy = 2r\, dr$. With these substitutions, equation (A5) becomes

$$J(n;\eta) = \exp\left(\frac{n}{2}\right) \left(\frac{2}{n}\right)^{\frac{n+2\eta}{2}} \int_{r=0}^{r=\infty} r^{(n+2\eta-2)} \exp\left(-r^2\right)\, 2r\, dr \tag{A7}$$

$$J(n;\eta) = \exp\left(\frac{n}{2}\right) \left(\frac{2}{n}\right)^{\frac{n+2\eta}{2}} 2 \int_{r=0}^{r=\infty} r^{(n+2\eta-1)} \exp\left(-r^2\right) dr. \tag{A8}$$

Inspection of a table of definite integrals [*Zwillinger*, 1996] shows that

$$J(n;\eta) = \exp\left(\frac{n}{2}\right)\left(\frac{2}{n}\right)^{\frac{n+2\eta}{2}}\Gamma\left(\frac{n+2\eta}{2}\right), \qquad \text{(A9)}$$

where the definition and properties of the gamma function (Γ) are discussed by *Arfken and Weber* [1995]. One example of the utility of $J(n;\eta)$ concerns the total electron content of a Chapman layer. The total electron content of a Chapman layer, such as the M2 layer, equals $N_0 L J(1; 0)$ (equations (8) and (A1)), where $J(1;0)$ equals $\exp(0.5)\sqrt{2}\,\Gamma(0.5)$, which equals $\exp(0.5)\sqrt{2\pi}$ or 4.133.

[49] **Acknowledgments.** P.W. acknowledges three thoughtful reviews, as well as productive discussions with members of the Living With a Star Targeted Research and Technology "Extreme space weather events in the solar system" Focus Team led by Yingjuan Ma. This work was partially supported by NASA grant NNX08AP96G.

References

Acuña, M. H., et al. (1999), Global distribution of crustal magnetization discovered by the Mars Global Surveyor MAG/ER Experiment, *Science*, *284*, 790–793, doi:10.1126/science.284.5415.790.

Acuña, M. H., et al. (2001), Magnetic field of Mars: Summary of results from the aerobraking and mapping orbits, *J. Geophys. Res.*, *106*, 23,403–23,418, doi:10.1029/2000JE001404.

Arfken, G. B., and H. J. Weber (1995), *Mathematical Methods for Physicists*, 4th ed., Academic Press, San Deigo, Calif.

Armand, N. A., V. M. Smirnov, and T. Hagfors (2003), Distortion of radar pulses by the Martian ionosphere, *Radio Sci.*, *38*(5), 1090, doi:10.1029/2002RS002849.

Blaunstein, N., and E. Plohotniuc (2008), *Ionosphere and Applied Aspects of Radio Communication and Radar*, CRC Press, Boca Raton, Fla.

Bougher, S. W., S. Engel, D. P. Hinson, and J. M. Forbes (2001), Mars Global Surveyor Radio Science electron density profiles: Neutral atmosphere implications, *Geophys. Res. Lett.*, *28*, 3091–3094, doi:10.1029/2001GL012884.

Brain, D. A., F. Bagenal, M. H. Acuña, and J. E. P. Connerney (2003), Martian magnetic morphology: Contributions from the solar wind and crust, *J. Geophys. Res.*, *108*(A12), 1424, doi:10.1029/2002JA009482.

Brain, D. A., R. J. Lillis, D. L. Mitchell, J. S. Halekas, and R. P. Lin (2007), Electron pitch angle distributions as indicators of magnetic field topology near Mars, *J. Geophys. Res.*, *112*, A09201, doi:10.1029/2007JA012435.

Brain, D. A., G. T. Delory, R. J. Lillis, J. G. Luhmann, S. W. Bougher, and C. D. Parkinson (2009), Energy deposition by energetic protons in the upper atmosphere of Mars, *Eos Trans. AGU*, *90*(52), Fall Meet. Suppl., Abstract P11B-1215.

Budden, K. G. (1985), *The Propagation of Radio Waves*, Cambridge Univ. Press, Cambridge, U. K.

Chapman, S. (1931a), The absorption and dissociative or ionizing effect of monochromatic radiation in an atmosphere on a rotating Earth, *Proc. Phys. Soc.*, *43*, 26–45.

Chapman, S. (1931b), The absorption and dissociative or ionizing effect of monochromatic radiation in an atmosphere on a rotating Earth, part II. Grazing incidence, *Proc. Phys. Soc.*, *43*, 483–501.

Chen, R. H., T. E. Cravens, and A. F. Nagy (1978), The Martian ionosphere in light of the Viking observations, *J. Geophys. Res.*, *83*, 3871–3876.

Chicarro, A., P. Martin, and R. Trautner (2004), The Mars Express mission: An overview, in *Mars Express: The Scientific Payload*, *ESA Spec. Publ. Ser.*, vol. SP-1240, edited by A. Wilson, pp. 3–16, Eur. Space Agency, Paris. (Available online at http://sci.esa.int/science-e/www/object/index.cfm?fobjectid=34885.)

Christou, A. A., J. Vaubaillon, and P. Withers (2007), The dust trail complex of 79P/du Toit-Hartley and meteor outbursts at Mars, *Astron. Astrophys.*, *471*, 321–329.

Crisp, J. A., M. Adler, J. R. Matijevic, S. W. Squyres, R. E. Arvidson, and D. M. Kass (2003), Mars Exploration Rover mission, *J. Geophys. Res.*, *108*(E12), 8061, doi:10.1029/2002JE002038.

Crosby, N., V. Bothmer, R. Facius, J. Grießmeier, X. Moussas, M. Panasyuk, N. Romanova, and P. Withers (2008), Interplanetary space weather and its planetary connection, *Space Weather*, *6*, S01003, doi:10.1029/2007SW000361.

Edwards, C. D., T. C. Jedrey, A. S. Devereaux, R. DePaula, and M. Dapore (2003), The Electra proximity link payload for Mars relay telecommunications and navigation, paper presented at 54th International Astronautical Congress, Am. Inst. of Aeronaut. and Astronaut., Bremen, Germany, 29 Sept. to 3 Oct. (Available at http://hdl.handle.net/2014/7832.)

El-Rabbany, A. (2002), *Introduction to GPS: The Global Positioning System*, Artech House, Boston.

Espley, J. R., W. M. Farrell, D. A. Brain, D. D. Morgan, B. Cantor, J. J. Plaut, M. H. Acuña, and G. Picardi (2007), Absorption of MARSIS radar signals: Solar energetic particles and the daytime ionosphere, *Geophys. Res. Lett.*, *34*, L09101, doi:10.1029/2006GL028829.

Foullon, C., N. Crosby, and D. Heynderickx (2005), Toward interplanetary space weather: Strategies for manned missions to Mars, *Space Weather*, *3*, S07004, doi:10.1029/2004SW000134.

Fox, J. L. (2004), Response of the Martian thermosphere/ionosphere to enhanced fluxes of solar soft X rays, *J. Geophys. Res.*, *109*, A11310, doi:10.1029/2004JA010380.

Fox, J. L., and K. E. Yeager (2006), Morphology of the near-terminator Martian ionosphere: A comparison of models and data, *J. Geophys. Res.*, *111*, A10309, doi:10.1029/2006JA011697.

Fox, J. L., J. F. Brannon, and H. S. Porter (1993), Upper limits to the nightside ionosphere of Mars, *Geophys. Res. Lett.*, *20*, 1339–1342, doi:10.1029/93GL01349.

Graf, J. E., R. W. Zurek, H. J. Eisen, B. Jai, M. D. Johnston, and R. Depaula (2005), The Mars Reconnaissance Orbiter Mission, *Acta Astronaut.*, *57*, 566–578, doi:10.1016/j.actaastro.2005.03.043.

Gurnett, D. A., and A. Bhattacharjee (2005), *Introduction to Plasma Physics: With Space and Laboratory Applications*, Cambridge Univ. Press, New York.

Gurnett, D. A., et al. (2005), Radar soundings of the ionosphere of Mars, *Science*, *310*, 1929–1933, doi:10.1126/science.1121868.

Gurnett, D. A., et al. (2008), An overview of radar soundings of the Martian ionosphere from the Mars Express spacecraft, *Adv. Space Res.*, *41*, 1335–1346, doi:10.1016/j.asr.2007.01.062.

Haider, S. A., M. A. Abdu, I. S. Batista, J. H. Sobral, X. Luan, E. Kallio, W. C. Maguire, M. I. Verigin, and V. Singh (2009), D, E, and F layers in the daytime at high-latitude terminator ionosphere of Mars: Comparison with Earth's ionosphere using COSMIC data, *J. Geophys. Res.*, *114*, A03311, doi:10.1029/2008JA013709.

Hake, R. D., and A. V. Phelps (1967), Momentum-transfer and inelastic-collision cross sections for electrons in O_2, CO, and CO_2, *Phys. Rev.*, *158*, 70–84, doi:10.1103/PhysRev.158.70.

Hanson, W. B., S. Sanatani, and D. R. Zuccaro (1977), The Martian ionosphere as observed by the Viking retarding potential analyzers, *J. Geophys. Res.*, *82*, 4351–4363.

Hargreaves, J. K. (1992), *The Solar-Terrestrial Environment*, Cambridge Univ. Press, New York.

Kliore, A. J., et al. (2004), Cassini radio science, *Space Sci. Rev.*, *115*, 1–70, doi:10.1007/s11214-004-1436-y.

Leblanc, F., J. G. Luhmann, R. E. Johnson, and E. Chassefiere (2002), Some expected impacts of a solar energetic particle event at Mars, *J. Geophys. Res.*, *107*(A5), 1058, doi:10.1029/2001JA900178.

Melnik, O., and M. Parrot (1999), Propagation of electromagnetic waves through the Martian ionosphere, *J. Geophys. Res.*, *104*, 12,705–12,714, doi:10.1029/1999JA900100.

Mendillo, M., X. Pi, S. Smith, C. Martinis, J. Wilson, and D. Hinson (2004), Ionospheric effects upon a satellite navigation system at Mars, *Radio Sci.*, *39*, RS2028, doi:10.1029/2003RS002933.

Mendillo, M., P. Withers, D. Hinson, H. Rishbeth, and B. Reinisch (2006), Effects of solar flares on the ionosphere of Mars, *Science*, *311*, 1135–1138, doi:10.1126/science.1122099.

Molina-Cuberos, G. J., H. Lichtenegger, K. Schwingenschuh, J. J. López-Moreno, and R. Rodrigo (2002), Ion-neutral chemistry model of the lower ionosphere of Mars, *J. Geophys. Res.*, *107*(E5), 5027, doi:10.1029/2000JE001447.

Molina-Cuberos, G. J., O. Witasse, J.-P. Lebreton, R. Rodrigo, and J. J. López-Moreno (2003), Meteoric ions in the atmosphere of Mars, *Planet. Space Sci.*, *51*, 239–249.

Morgan, D. D., D. A. Gurnett, D. L. Kirchner, R. L. Huff, D. A. Brain, W. V. Boynton, M. H. Acuña, J. J. Plaut, and G. Picardi (2006), Solar control of radar wave absorption by the Martian ionosphere, *Geophys. Res. Lett.*, *33*, L13202, doi:10.1029/2006GL026637.

Morgan, D. D., et al. (2010), Radar absorption due to a corotating interaction region encounter with Mars detected by MARSIS, *Icarus*, *206*, 95–103, doi:10.1016/j.icarus.2009.03.008.

Nicholson, W. P., G. Gronoff, J. Lilensten, A. D. Aylward, and C. Simon (2009), A fast computation of the secondary ion production in the ionosphere of Mars, *Mon. Not. R. Astron. Soc.*, *400*, 369–382, doi:10.1111/j.1365-2966.2009.15463.x.

Nielsen, E., D. D. Morgan, D. L. Kirchner, J. Plaut, and G. Picardi (2007), Absorption and reflection of radio waves in the Martian ionosphere, *Planet. Space Sci.*, *55*, 864–870, doi:10.1016/j.pss.2006.10.005.

Owen, T. (1992), The composition and early history of the atmosphere of Mars, in *Mars*, edited by H. H. Kieffer et al., pp. 818–834, Univ. of Ariz. Press, Tucson, Ariz.

Pätzold, M., S. Tellmann, B. Häusler, D. Hinson, R. Schaa, and G. L. Tyler (2005), A sporadic third layer in the ionosphere of Mars, *Science*, *310*, 837–839, doi:10.1126/science.1117755.

Pesnell, W. D., and J. Grebowsky (2000), Meteoric magnesium ions in the Martian atmosphere, *J. Geophys. Res.*, *105*, 1695–1708, doi:10.1029/1999JE001115.

Picardi, G., et al. (2004), MARSIS: Mars Advanced Radar for subsurface and ionosphere sounding, in *Mars Express: The Scientific Payload*, *ESA Spec. Publ. Ser.*, vol. SP-1240, edited by A. Wilson, pp. 51–69, Eur. Space Agency, Paris. (Available at http://sci.esa.int/science-e/www/object/index.cfm?fobjectid=34885.)

Ratcliffe, J. A. (1959), *The Magneto-Ionic Theory and Its Applications to the Ionosphere*, Cambridge Univ. Press, Cambridge, U. K.

Rawer, K. (1993), *Wave Propagation in the Ionosphere*, Springer, New York.

Rees, M. H., and R. A. Jones (1973), Time dependent studies of the aurora—Part II. Spectroscopic morphology, *Planet. Space Sci.*, *21*, 1213–1235, doi:10.1016/0032-0633(73)90207-9.

Reinisch, B. W., et al. (2000), The Radio Plasma Imager investigation on the IMAGE spacecraft, *Space Sci. Rev.*, *91*, 319–359.

Rishbeth, H., and O. K. Garriott (1969), *Introduction to Ionospheric Physics*, Academic Press, New York.

Roncoli, R. B., and J. N. Ludwinski (2002), Mission design overview for the Mars Exploration Rover mission, paper presented at 2002 Astrodynamics Specialist Conference, Am. Inst. of Aeronaut. and Astronaut./Am. Astron. Soc., Monterey, Calif., 5–8 Aug. (Available at http://hdl.handle.net/2014/9667.)

Safaeinili, A., W. Kofman, J. Nouvel, A. Herique, and R. L. Jordan (2003), Impact of Mars ionosphere on orbital radar sounder operation and data processing, *Planet. Space Sci.*, *51*, 505–515.

Saunders, R. S., et al. (2004), 2001 Mars Odyssey mission summary, *Space Sci. Rev.*, *110*, 1–36, doi:10.1023/B:SPAC.0000021006.84299.18.

Schunk, R. W., and A. F. Nagy (2000), *Ionospheres*, Cambridge Univ. Press, New York.

Seu, R., D. Biccari, R. Orosei, L. V. Lorenzoni, R. J. Phillips, L. Marinangeli, G. Picardi, A. Masdea, and E. Zampolini (2004), SHARAD: The MRO 2005 shallow radar, *Planet. Space Sci.*, *52*, 157–166, doi:10.1016/j.pss.2003.08.024.

Tyler, G. L., G. Balmino, D. P. Hinson, W. L. Sjogren, D. E. Smith, R. A. Simpson, S. W. Asmar, P. Priest, and J. D. Twicken (2001), Radio science observations with Mars Global Surveyor: Orbit insertion through one Mars year in mapping orbit, *J. Geophys. Res.*, *106*, 23,327–23,348, doi:10.1029/2000JE001348.

Witasse, O., J. Nouvel, J. Lebreton, and W. Kofman (2001), HF radio wave attenuation due to a meteoric layer in the atmosphere of Mars, *Geophys. Res. Lett.*, *28*, 3039–3042, doi:10.1029/2001GL013164.

Withers, P. (2009), A review of observed variability in the dayside ionosphere of Mars, *Adv. Space Res.*, *44*, 277–307, doi:10.1016/j.asr.2009.04.027.

Withers, P., M. Mendillo, D. P. Hinson, and K. Cahoy (2008), Physical characteristics and occurrence rates of meteoric plasma layers detected in the Martian ionosphere by the Mars Global Surveyor Radio Science Experiment, *J. Geophys. Res.*, *113*, A12314, doi:10.1029/2008JA013636.

Zhang, M. H. G., J. G. Luhmann, and A. J. Kliore (1990), An observational study of the nightside ionospheres of Mars and Venus with radio occultation methods, *J. Geophys. Res.*, *95*, 17,095–17,102, doi:10.1029/JA095iA10p17095.

Zurek, R. W., and S. E. Smrekar (2007), An overview of the Mars Reconnaissance Orbiter (MRO) science mission, *J. Geophys. Res.*, *112*, E05S01, doi:10.1029/2006JE002701.

Zurek, R. W., J. R. Barnes, R. M. Haberle, J. B. Pollack, J. E. Tillman, and C. B. Leovy (1992), Dynamics of the atmosphere of Mars, in *Mars*, edited by H. H. Kieffer et al., pp. 835–933, Univ. of Ariz. Press, Tucson, Ariz.

Zwillinger, D. (1996), *CRC Standard Mathematical Tables and Formulae*, 30th ed., CRC Press, New York.

P. Withers, Center for Space Physics, Boston University, 725 Commonwealth Ave., Boston, MA 02215, USA. (withers@bu.edu)